

# Non-invasive and depth-free temperature monitoring using MR thermometry in plasmonic photothermal therapy using gold nanorods

Seung-Hyun Yang<sup>a</sup>, Kiyoung Jeong<sup>b</sup>, Jaemoon Yang<sup>a</sup>, Hye Young Son<sup>b</sup>, Jin-Suck Suh<sup>a,c</sup>,  
Yong-Min Huh<sup>a,b,c,d,\*\*</sup>, Seung Jae Oh<sup>b,\*</sup>

<sup>a</sup> Department of Radiology, College of Medicine, Yonsei University, Seoul 03722, Republic of Korea

<sup>b</sup> YUHS-KRIBB Medical Convergence Research Institute, College of Medicine, Seoul 03722, Republic of Korea

<sup>c</sup> Severance Biomedical Science Institute, College of Medicine, Yonsei University, Seoul 03722, Republic of Korea

<sup>d</sup> Department of Biochemistry & Molecular Biology, College of Medicine, Yonsei University, Seoul 03722, Republic of Korea

## ARTICLE INFO

### Keywords:

Plasmonic photothermal therapy  
Gold nanorods  
MR thermometry  
Tumor phantom  
Heat transfer

## ABSTRACT

This study used magnetic resonance (MR) thermometry to investigate the temperature increases and thermal transfer that occur during plasmonic photothermal therapy (PTT) with gold nanorods (GNRs). An artificial tumor phantom made of agarose gel containing GNRs was heated by irradiation with an 808 nm laser. The MR thermometry visualized the conditions: a well-localized temperature distribution with suppressed thermal diffusion that depended on laser power and irradiation time. A tumor phantom model was implanted in mice, and MR thermometry evaluated the temperature change in the presence and absence of GNRs and the thermal transfer into the surrounding tissues. That experiment showed that MR thermometry can be a useful tool for monitoring PTT. These results suggest that MR temperature measurement could help to establish ideal laser irradiation conditions in GNR-mediated PTT, and that it has great potential for visualizing local photothermal induction and evaluating therapeutic effects.

## 1. Introduction

Loco-regional thermal ablation of tumors is a conventional local therapy that uses high temperature to induce tumor cell apoptosis or coagulative necrosis. It has many potential benefits over surgery, including lower morbidity, increased preservation of surrounding normal tissues, reduced cost, and shorter hospitalization time [1,2]. The loco-regional thermal ablation techniques that are clinically available are LITT (laser-induced thermal therapy), RFA (radiofrequency ablation), and HIFU (high-intensity focused ultrasound), which use a laser, radio frequency, and ultrasound, respectively, as the heat source. The challenge in using such techniques is to eliminate abnormal tissue without causing damage to the surrounding normal, healthy tissue. Thus, temperature monitoring and complex simulations that determine the intensity, and shape of the thermal source have been conducted to localize the appropriate amount of heat at the target region [3–5]. Despite such careful attention to the target, treatment of tumor tissues that are irregularly scattered or in complicated radial shapes often

damages healthy tissues. That problem can be addressed using therapeutic techniques such as target-specific functional nanoparticles, also known as nanoprobes. When surface plasmon resonance occurs on the nanoparticle surfaces under laser irradiation, only the targeted tumor tissue containing the nanoparticles is heated, protecting the normal region from damage regardless of tumor shape or distribution [6]. In this regard, plasmonic photothermal therapy (PTT) has been studied. PTT combines laser therapy and nanoparticle technology to enable tumor-specific heating. Nanoparticles with tumor-specific molecules, such as an antibody or aptamer, enable selective tumor treatment by PTT. Gold nanorods (GNRs) have been widely used in PTT studies. GNRs can support a higher-absorption cross-sectional area of near infrared waves per unit volume than other types of nanoparticles, and they exhibit a much narrower linewidth than spherical nanoparticles at similar resonance frequencies due to their reduced radiation damping effect [7]. In addition, GNRs have been identified as optimal nanoparticles because they can be synthesized in bulk, have broadly tunable plasmon resonance, and allow easy surface modification. Various cancer

\* Corresponding author.

\*\* Corresponding author. Department of Radiology, College of Medicine, Yonsei University, Seoul 03722, Republic of Korea.

E-mail addresses: [yhmuh@yuhs.ac](mailto:yhmuh@yuhs.ac) (Y.-M. Huh), [issac@yuhs.ac](mailto:issac@yuhs.ac) (S.J. Oh).

<https://doi.org/10.1016/j.cap.2022.10.004>

Received 27 June 2022; Received in revised form 1 October 2022; Accepted 5 October 2022

Available online 13 October 2022

1567-1739/© 2022 Korean Physical Society. Published by Elsevier B.V. All rights reserved.

treatment and imaging studies using GNRs have been conducted [8–11]. Although PTT cancer treatment using GNRs has been quite effective, accurate temperature monitoring around the GNRs is required to minimize unintended effects on nearby normal cells. Many studies have been performed to monitor the temperature distribution in regions with and without nanoprobes using visible, mid-infrared, terahertz, and magnetic resonance (MR) imaging [12–16]. Among those options, MR thermometry have been spotlighted as a non-invasive, non-depth-limited tool that does not require ionizing radiation, offers an excellent anatomical resolution, and is useful in all scan directions [2]. MR imaging can measure the proton resonant frequency change of hydrogen proton in water molecules when the temperature of water was changed. MR thermometry is not limited to surfaces, but can measure internal temperature and profile thermal transfer using several methods including proton resonance frequency, proton density, magnetization transfer, and diffusion coefficient [17–19]. MR thermometry is suitable for LITT and PTT applications because they do not interfere with the laser. Even with HIFU, MRI-compatible multi-element ultrasound transducers can be used to provide spatial control of the heating zone [2]. On the other hand, RFA is not recommended with MR thermometry unless proper filtering is implemented because interference between the RF and MR systems is a serious concern [20]. Although it is important to understand the transfer temperature trends around the tumor, previous MR thermometry studies in PTT have mostly used spherical gold nanoparticles; no previous studies have used GNRs [21,22]. Accurate temperature monitoring studies are needed because GNRs can absorb 3–5 times more light energy from plasmon resonance than spherical gold nanoparticles at the same gold mass [23]. This study used MR thermometry to measure the photothermally induced temperature distribution in a GNR-implanted tumor phantom and a tumor phantom-implanted mouse model. The contours of each temperature distribution within specially selected ranges in the tumor phantom are displayed as binary temperature maps. Analysis of those binary temperature maps shows that MR thermometry can be used to optimize laser irradiation conditions. The temperature distribution and thermal transfer of the GNR-implanted tumor phantoms were verified *in vivo* using MR thermometry in mice with implanted tumor phantoms. Those experiments confirmed the different tendencies of temperature increases and decreases depending on the presence or absence of GNRs and showed that it is possible to monitor differences in the degree of heat transfer into surrounding tissue. These results demonstrate that the MR thermometry has potential as a monitoring system to non-invasively confirm the therapeutic effect of PTT without depth limitation and to minimize the side effects to normal tissue.

## 2. Materials and methods

### 2.1. Materials

Hexadecyltrimethylammonium bromide solution, sodium borohydride solution, gold(III) chloride trihydrate, ascorbic acid solution, and silver nitrate solution were purchased from Sigma-Aldrich (MO, USA). Agarose powder was purchased from Gendepot (TX, USA). Ultrapure deionized water was used for all syntheses. All other chemicals and reagents were analytical grade.

### 2.2. Preparation of GNR-implanted tumor phantom

GNRs with surface plasmon resonance waves of 808 nm in water were synthesized using a seed-mediated growth technique in a previously published protocol with some modifications [24,25]. The 50  $\mu\text{M}$  GNRs were included in a cylindrical tumor phantom with a height of 1 cm and diameter of 8 mm that was located more than 2 mm from the top of a rectangular phantom. A 2-mm layer of agarose covered the top surface of the phantom, as shown in Fig. 1.

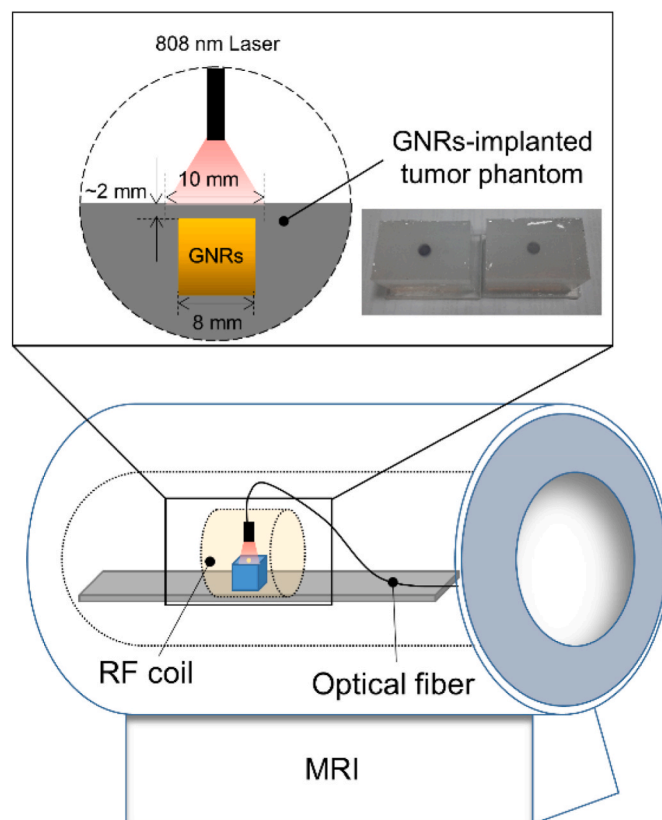


Fig. 1. Schematic image of the experiments.

### 2.3. Laser irradiation

Throughout the experiments, laser irradiation was implemented at a room temperature of  $\sim 20^\circ\text{C}$  [26]. A continuous wave laser beam of 808 nm was guided to the phantom via a 10-m optical fiber, as shown in Fig. 1. The laser irradiation had a diameter of 10 mm, larger than the tumor phantom size, with power densities of  $3.8\text{ W/cm}^2$  and  $6.4\text{ W/cm}^2$ .

### 2.4. MR thermometry

MR thermometry was implemented at a room temperature of  $\sim 20^\circ\text{C}$ . The MR signals of the tumor phantom were obtained using an 8ch HD T/R hand coil (GE Healthcare, IL, USA). Images for the thermo map were acquired by fast Spoiled Gradient echo (fSPGR) pulse sequence on a 3.0 T GE Discovery MR750 scanner. The parameters were  $\text{TR/TE} = 3500/79.6$ , image matrix =  $256 \times 256$ , slice thickness = 4 mm. The acquisition time per slide was approximately 10 s, and 6 and 24 slides were obtained before and after laser irradiation, respectively. The proton resonance frequency method was used to reconstruct the temperature maps, and the algorithm was executed by IDL (Version 8.2, Exelis Visual Information Solutions, Inc., VA, USA). The temperature map was analyzed considering the specific temperature boundaries inside and outside the phantom.

### 2.5. Animal care and *in vivo* MR thermometry

Five-week-old male athymic BALB/c nude mice (Orient Bio, Korea) were used for the tumor phantom experiments. The mice were retained in microisolator cages under sterile conditions and observed for at least 1 week before study initiation to ensure their proper health. Temperature, lighting, and humidity were controlled centrally. All experimental procedures were carried out in accordance with the guidelines of the Institutional Animal Care and Use Committee and approved by Yonsei

University College of Medicine. Before the experiments, all mice were anesthetized with 2% isoflurane. Tumor phantoms mixed with Matrigel® matrix (Corning, AZ, USA) and 50  $\mu\text{M}$  GNRs were prepared and transplanted onto the left thigh of each mouse. For the control group, only Matrigel was transplanted without GNRs. After the Matrigel was sufficiently hardened by mouse body temperature, MR thermometry was performed during laser irradiation. The MR thermometry measured the temperature every 10 s, and the laser irradiation lasted 250 s.

### 3. Results

#### 3.1. Temperature mapping after laser irradiation

To confirm the non-invasive temperature measurement capability of MR thermometry, tumor phantoms with and without GNRs were prepared using agarose gel and were irradiated with a laser, and then the temperature inside each tumor phantom was measured using MR thermometry. Fig. 2a and b show the T2 MR images of the tumor-mimicking phantoms with and without GNRs before laser irradiation. When a laser with 6.4  $\text{W}/\text{cm}^2$  of power was used for 140 s on both phantoms, the conventional T2 MR images of the GNR phantom and GNR-free phantom did not differ significantly. However, when image reconstruction for temperature was applied, a significant temperature difference was clear, as shown in Fig. 2c and d. The maximum temperature increase for the GNR-implanted tumor phantom was 16  $^{\circ}\text{C}$ , whereas the tumor phantom without GNRs experienced only a very slight temperature increase due to the laser irradiation itself. As shown in Fig. 2f, in the tumor phantoms with GNRs, thermal transfer was observed from the center to the outside unlike Fig. 2e tumor phantom without GNRs.

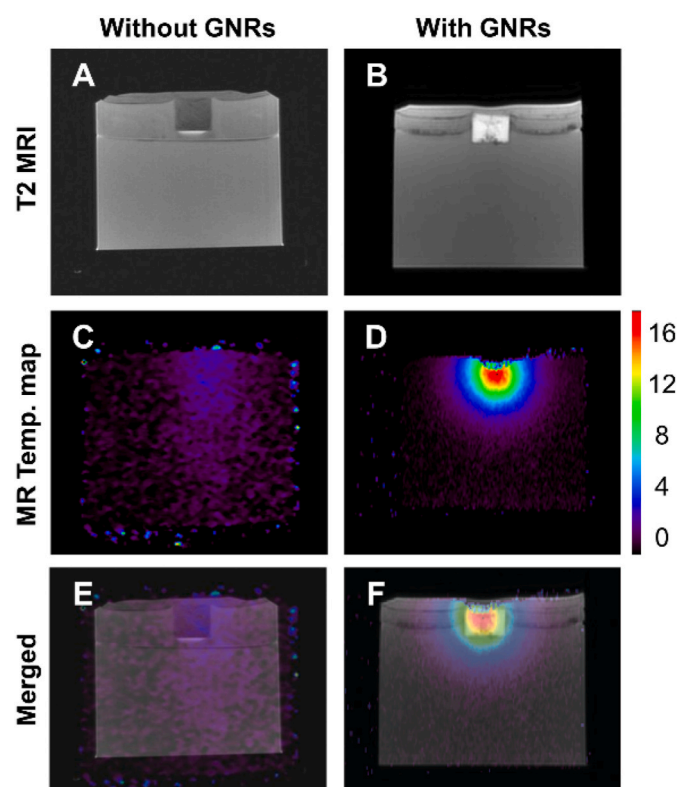


Fig. 2. MR images and temperature map of the tumor phantoms. (a) and (b) T2 MR images of the tumor phantoms, (c) and (d) temperature maps of the tumor phantoms after laser irradiation, (e) and (f) merged images of the tumor phantoms. The color bar scale is temperature difference ( $^{\circ}\text{C}$ ). (For interpretation of the references to color in this figure legend, the reader is referred to the Web version of this article.)

#### 3.2. Characterization of heat transfer profiles

Ideally, PTT increases the temperature of the target area as much as intended and prevents thermal damage in the surrounding area by suppressing temperature changes there. Therefore, the boundary of each temperature range must be carefully monitored during heat transfer in both the normal and abnormal regions. Because the effectiveness of PTT is highly dependent on thermal dose, 25 various temperatures were used as guidelines, and a binary temperature contour map was applied to characterize the temperature and thermal transfer around the tumor phantom. Fig. 3a shows the changes in areas of the GNR-implanted tumor phantom in which the temperature increased by 6, 8, and 10  $^{\circ}\text{C}$  upon irradiation with a 3.8  $\text{W}/\text{cm}^2$  laser. After 80 s of laser irradiation, most areas of the tumor phantom had increased by 6  $^{\circ}\text{C}$  but had not been affected to the extent to increase the temperature by 8 or 10  $^{\circ}\text{C}$ . After 300 s, the heat increase was in the 6 and 8  $^{\circ}\text{C}$  range. Fig. 3b shows the results from irradiation with a 6.4  $\text{W}/\text{cm}^2$  laser. Most of the tumor phantom had increased by 10  $^{\circ}\text{C}$  in 80 s. The area that increased by 14  $^{\circ}\text{C}$  was very wide, and the 6  $^{\circ}\text{C}$  increase had begun to affect the surrounding area. The area with a 6  $^{\circ}\text{C}$  increase was much larger than the tumor phantom after 300 s, but the area with a 14  $^{\circ}\text{C}$  increase remained well localized in the phantom, with no significant change from 80 s. These results show that laser power and irradiation time should vary depending on the temperature increase needed in the irradiation site, and that MR thermometry monitoring is an important tool for controlling heat transfer into normal tissues.

#### 3.3. Assessment of heat localization efficiency

To evaluate the localization efficiency of various temperature ranges according to laser power and exposure time, the tumor phantom area was divided into 4 areas, as shown in Fig. 4a: all regions in which the temperature increased (area 1), the regions with a temperature increase that corresponded to the tumor phantom (area 2), the regions outside the tumor phantom with a temperature increase (area 3), and the tumor phantom regions in which the temperature did not increase (area 4). Areas 1 and 2 expanded over time during laser irradiation, but it was predicted that there would be no further change once area 2 was equal in size to the area of the tumor phantom. The temperature in area 3, outside the tumor phantom, should increase after that in all other tested areas. At the start of the experiment, area 4 was the same as the tumor phantom, and it was expected to decrease during laser irradiation. Therefore, the optimal treatment condition, in which heat is concentrated in the tumor site and transfer to the periphery is suppressed, would show similar increases in areas 1 and 2 and approaching contact of graphs of areas 3 and 4 during laser irradiation. With laser irradiation at 3.8  $\text{W}/\text{cm}^2$ , the areas in which the temperature increased by 6 and 8  $^{\circ}\text{C}$  were wider than the tumor phantom, and there was heat transfer to the outer area (Fig. 4b). On the other hand, the area in which the temperature increased by 10  $^{\circ}\text{C}$  was localized to the tumor phantom and remained nearly identical to areas 1 and 2. After 110 s of laser irradiation, areas 1 and 2 stopped showing significant changes, and areas 3 and 4 contacted each other. Thus, if a tumor is treated using the same conditions as the tumor phantom, laser irradiation of 110 s or more is required to increase the temperature by 10  $^{\circ}\text{C}$ . With the 6.4  $\text{W}/\text{cm}^2$  laser, thermal transfer occurred in both the 6 and 10  $^{\circ}\text{C}$  increase regions, which were wider than the 6 and 8  $^{\circ}\text{C}$  increase regions with 3.8  $\text{W}/\text{cm}^2$  laser irradiation. On the other hand, the area with a 14  $^{\circ}\text{C}$  increase remained well localized to the tumor phantom. The initial laser irradiation produced increases that almost matched those of areas 1 and 2. After 100 s of laser irradiation, areas 1 and 2 no longer showed significant changes; areas 3 and 4 contacted each other after 140 s of laser irradiation. Unlike the other conditions, the increase in area 3 was greatly suppressed. The MR thermometry showed that the 14  $^{\circ}\text{C}$  increase was well localized to the tumor phantom area under irradiation from a 6.8  $\text{W}/\text{cm}^2$  laser, and heat transfer to the periphery was suppressed

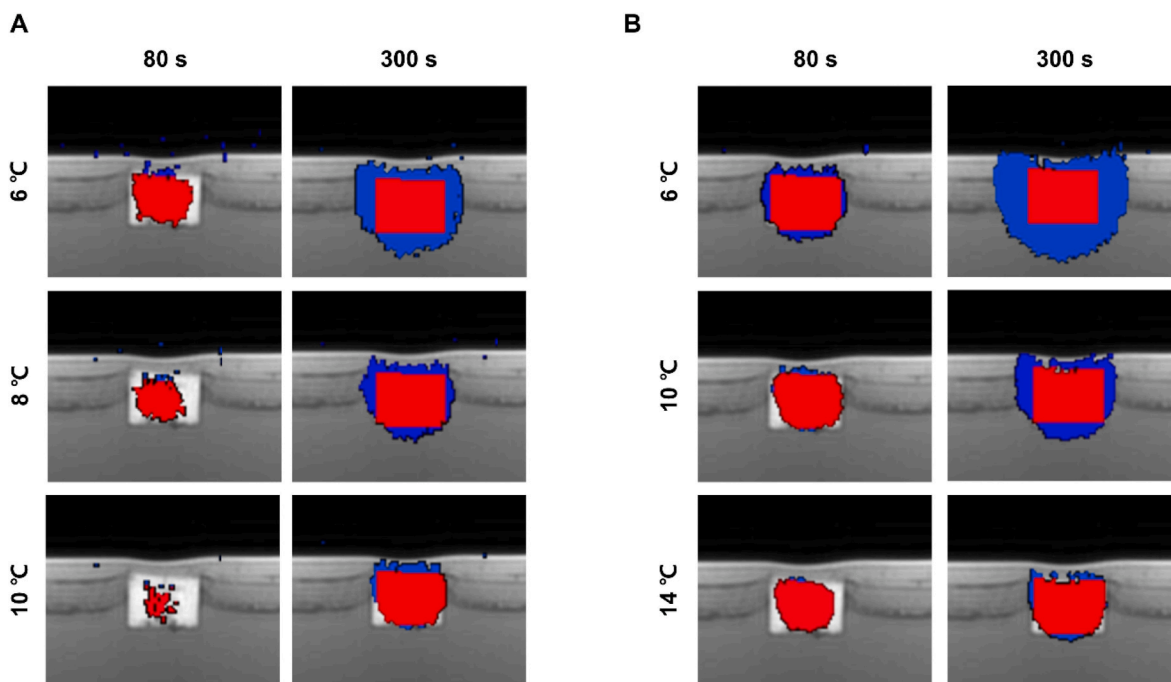


**Fig. 3.** MR thermometry of tumor phantoms with GNRs during laser irradiation. For each area, increases of 6, 8, and 10 °C were measured upon 3.8 W/cm<sup>2</sup> laser irradiation (a), and 6, 10, and 14 °C increases were measured upon 6.4 W/cm<sup>2</sup> laser irradiation (b), The red color means the area which temperature was higher than 6, 8, and 10 °C in the tumor phantom area, respectively. The blue color means the area which temperature was higher than 6, 8, and 10 °C out the tumor phantom area, respectively. (For interpretation of the references to color in this figure legend, the reader is referred to the Web version of this article.)

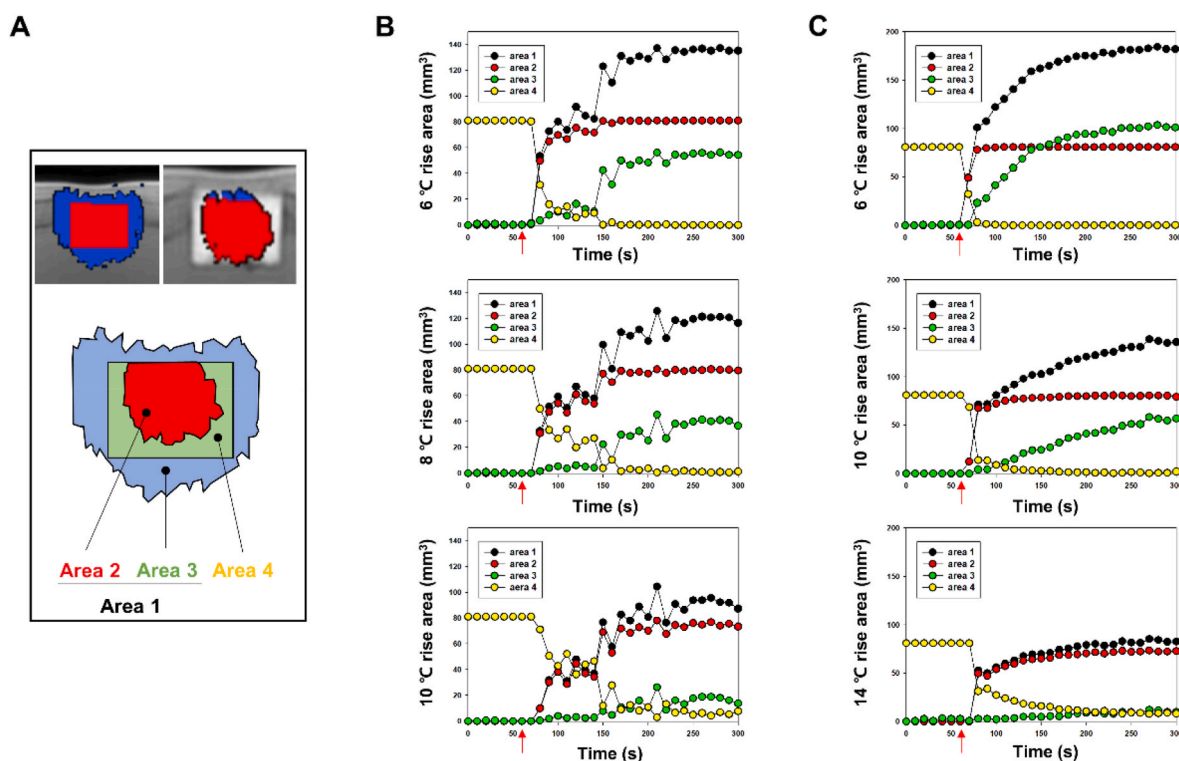


**Fig. 4.** Heat localization graph at various temperatures. The experimental area was divided into 4 regions (a). Areas increased by 6, 8, and 10 °C were measured upon 3.8 W/cm<sup>2</sup> laser irradiation (b). Areas increased by 6, 10, and 14 °C were measured upon 6.4 W/cm<sup>2</sup> laser irradiation (c). (Red arrow: laser irradiation onset). (For interpretation of the references to color in this figure legend, the reader is referred to the Web version of this article.)

(Fig. 4c). These MR thermometry results show that thermal transfer differs widely depending on set temperature and laser power. They also suggest that MR thermometry is a useful tool for monitoring these phenomena.

### 3.4. *In vivo* MR thermometry

To use MR thermometry to evaluate the temperatures, changes, and thermal transfer according to presence of GNRs and laser irradiation *in vivo*, a mouse experiment was conducted. Tumor phantoms were implanted in the left thighs of mice using Matrigel®, and the internal temperature change caused by laser irradiation was measured with MR thermometry (Fig. 5a). In the tumor phantoms with GNRs, the temperature increased rapidly after 50 s of laser irradiation but was concentrated in the GNR region (Fig. 5b). In the control tumor phantom, laser irradiation generated only weak heat that spread widely to the surrounding area. The control tumor phantom showed no significant temperature change for about 50 s after the start of laser irradiation, and then the temperature changed slowly to a maximum increase of 12.64 °C until the laser was turned off. The GNR-implanted tumor phantom increased rapidly in temperature after the start of laser irradiation, increased by 12.59 °C in 50 s, and then continued to a maximum increase of 26.19 °C until the laser was turned off. After turning off the laser, the temperature of the tumor phantom containing the GNRs decreased rapidly and was only 3.08 °C higher than the starting temperature after 700 s. In the control tumor phantom, on the other hand, the temperature decreased slowly even after the laser was turned off, and the temperature after 700 s was 7.94 °C above starting temperature (Fig. 5c). These results demonstrate that MR thermometry can precisely monitor heating of the target site and transfer of heat to the periphery of PTT using GNRs. It also suggests that MR thermometry is a useful tool for preventing unintended side effects in normal tissues.

### 4. Discussion

In PTT, monitoring the temperature and thermal transfer of the laser site is important to ensure treatment effectiveness and to reduce side effects. MRI is a non-invasive imaging technique that can acquire anatomical images without depth limitation and can be applied to precisely measure temperature change, location, and thermal transfer of PTT unlike conventional method of measuring the surface temperature. A tumor phantom of agarose gel and GNRs was placed in an MRI and

irradiated with a laser. A binary temperature map was applied at specific temperatures to evaluate changes in appropriate heat locations and transfer according to laser irradiation time and output. Areas with an increase of 6 or 8 °C showed rapid heat transfer into the surrounding tissue, even with low-power laser irradiation. The temperature maps show that the 10 and 14 °C increases occurred predominantly at the tumor phantom location, and heat transfer to the surroundings was suppressed. The tendency of thermal transfer from the inside to the surroundings is difficult to detect with typical temperature monitoring. These results suggest that when using PTT with GNRs, the tendency of heat transfer varies according to the required range and temperature, so it is necessary to precisely control the laser power and time, and MR thermometry can be useful in the process. In a murine *in vivo* experiment, non-invasive MR thermometry clearly confirmed the thermal transfer and temperature changes not only in the laser irradiated area, but also in the surrounding areas. MR thermometry made it possible to accurately and conveniently monitor the temperature increase rate, maximum temperature, and thermal transfer in the presence and absence of GNRs in the tumor phantom. To perform effective PTT, it is important to consider the temperature of the heat source and the environment surrounding the tumor. The MR thermometry is an excellent method for non-invasive monitoring of temperature inside and outside the tumor without depth limitation, and offers potential applications in a variety of hyperthermia.

### 5. Conclusion

In this study, we evaluated the temperature change of a tumor phantom PTT containing gold nanorods non-invasively without depth limitation using an MR thermometry. The temperature changes and thermal transfer of the tumor phantom by laser irradiation were shown through binary mapping. In this study, it was found with an MR thermometry that the tendency of heat transfer in the tumor phantom was different depending on the laser power and irradiation time.

In the mouse model, it was confirmed that the tendency of temperature rises and heat transfer in the tumor phantom using GNRs was different from that in the tumor phantom without GNRs. Therefore, it

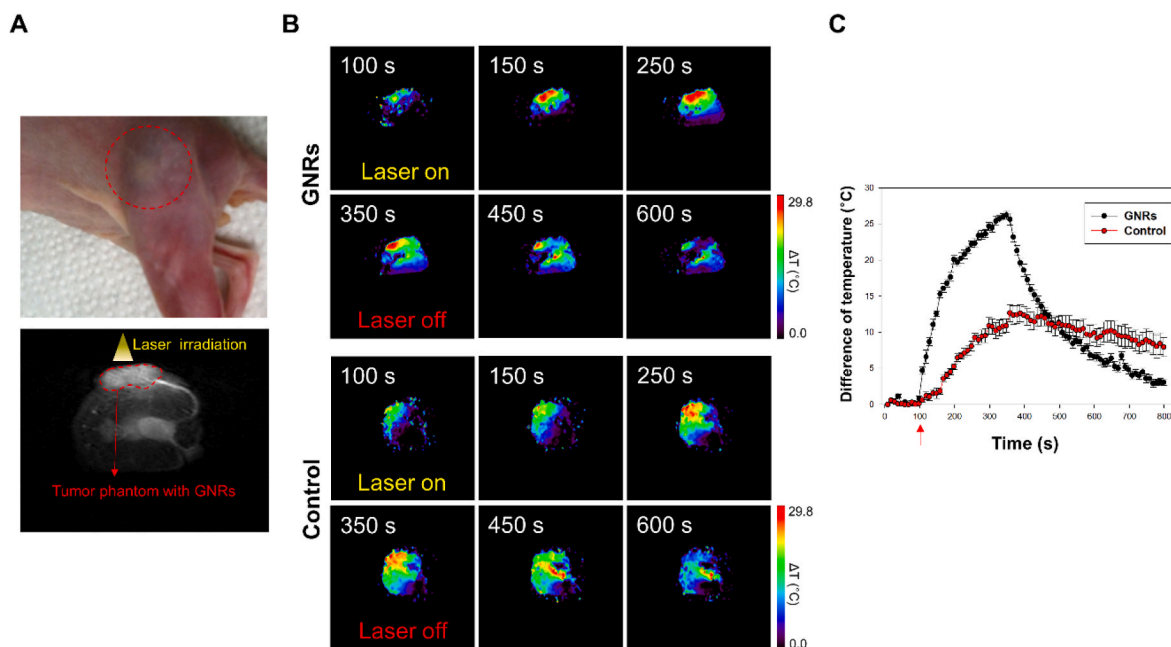


**Fig. 5.** Temperature changes in mouse tumor phantoms upon laser irradiation, measured using MR thermometry. Photo and T2 MR image of mouse tumor phantom (a), MR thermometry upon 16 W/cm<sup>2</sup> laser irradiation (b), and a temperature difference graph of mouse tumor phantoms over time (c). The color bar is temperature difference. (Red arrow: laser irradiation onset). (For interpretation of the references to color in this figure legend, the reader is referred to the Web version of this article.)

can be used in real time to suppress side effects to normal tissues in simultaneous diagnostic treatment using PTT and gold nanorods [27, 28]. MR thermometry show the potential to monitor temperature changes in a variety of thermal treatments. In addition, the change of the binary map in temperature transfer could be utilized for PPT or heat treatment therapy evaluation based on the artificial intelligence.

#### Declaration of competing interest

The authors declare that they have no known competing financial interests or personal relationships that could have appeared to influence the work reported in this paper.

#### Acknowledgments

We thank to Yeogyong Lee of King's College London for proof of this manuscript. This study was supported by a National Research Foundation of Korea grant funded by the Korea government (NRF-2021R1A6A3A01086846 and Institute of Information & communications Technology Planning & evaluation(IITP) grant funded by the Korea government (MSIT) (2022-0-01044, Development of terahertz wave-based real-time intelligent brain tumor diagnosis system and technology).

#### References

- [1] K.F. Chu, D.E. Dupuy, Thermal ablation of tumours: biological mechanisms and advances in therapy, *Nat. Rev. Cancer* 14 (2014) 199–208.
- [2] V. Rieke, K. Butts Pauly, MR thermometry, *J. Magn. Reson. Imag. : JMRI* 27 (2008) 376–390.
- [3] F.A. Jolesz, *Intraoperative Imaging and Image-Guided Therapy*, Springer, New York, 2014.
- [4] S.N. Goldberg, G.S. Gazelle, P.R. Mueller, Thermal ablation therapy for focal malignancy: a unified approach to underlying principles, techniques, and diagnostic imaging guidance, *AJR. Am J. Roentgenol.* 174 (2000) 323–331.
- [5] P.K. Gupta, J. Singh, K.N. Rai, A numerical study on heat transfer in tissues during hyperthermia, *Math. Comput. Model.* 57 (2013) 1018–1037.
- [6] E.K. Lim, T. Kim, S. Paik, S. Haam, Y.M. Huh, K. Lee, Nanomaterials for theranostics: recent advances and future challenges, *Chem. Rev.* 115 (2015) 327–394.
- [7] C. Sönnichsen, T. Franzl, T. Wilk, G. von Plessen, J. Feldmann, O. Wilson, P. Mulvaney, Drastic reduction of plasmon damping in gold nanorods, *Phys. Rev. Lett.* 88 (2002), 077402.
- [8] T.B. Huff, L. Tong, Y. Zhao, M.N. Hansen, J.-X. Cheng, A. Wei, Hyperthermic effects of gold nanorods on tumor cells, *Nanomedicine* 2 (2007) 125–132.
- [9] E.M. Schuh, R. Portela, H.L. Gardner, C. Schoen, C.A. London, Safety and efficacy of targeted hyperthermia treatment utilizing gold nanorod therapy in spontaneous canine neoplasia, *BMC Vet. Res.* 13 (2017), 294–294.
- [10] T.S. Hauck, T.L. Jennings, T. Yatsenko, J.C. Kumaradas, W.C.W. Chan, Enhancing the toxicity of cancer chemotherapeutics with gold nanorod hyperthermia, *Adv. Mater.* 20 (2008) 3832–3838.
- [11] J. Choi, Y. Park, E.B. Choi, H.O. Kim, D.J. Kim, Y. Hong, S.H. Ryu, J.H. Lee, J. S. Suh, J. Yang, Y.M. Huh, S. Haam, Aptamer-conjugated gold nanorod for photothermal ablation of epidermal growth factor receptor-overexpressed epithelial cancer, *J. Biomed. Opt.* 19 (2014), 051203.
- [12] A.M. Gobin, M.H. Lee, N.J. Halas, W.D. James, R.A. Drezek, J.L. West, Near-infrared resonant nanoshells for combined optical imaging and photothermal cancer therapy, *Nano Lett.* 7 (2007) 1929–1934.
- [13] C.L. West, A.C.V. Doughty, K. Liu, W.R. Chen, Monitoring tissue temperature during photothermal therapy for cancer, *J BioX Res* 2 (2019) 159–168.
- [14] Y. Chen, S. Gnyawali, F. Wu, H. Liu, Y. Tesiram, A. Abbott, R. Towner, W. Chen, Magnetic resonance imaging guidance for laser photothermal therapy, *J. Biomed. Opt.* 13 (2008), 044033.
- [15] X. Meng, B. Zhang, Y. Yi, H. Cheng, B. Wang, Y. Liu, T. Gong, W. Yang, Y. Yao, H. Wang, W. Bu, Accurate and real-time temperature monitoring during MR imaging guided PTT, *Nano Lett.* 20 (2020) 2522–2529.
- [16] S.J. Oh, J. Kang, I. Maeng, J.-S. Suh, Y.-M. Huh, S. Haam, J.H. Son, Nanoparticle-enabled terahertz imaging for cancer diagnosis, *Opt Express* 17 (2009) 3469–3475.
- [17] J. MacFall, D.M. Prescott, E. Fullar, T.V. Samulski, Temperature dependence of canine brain tissue diffusion coefficient measured in vivo with magnetic resonance echo-planar imaging, *Int. J. Hyperther. : Off. Eur. J. Soc. Hyperthermic Oncol. North Am. Hyperther. Group.* 11 (1995) 73–86.
- [18] U. Kägebein, O. Speck, F. Wacker, B. Hensen, Motion correction in proton resonance frequency-based thermometry in the liver, *Top. Magn. Reson. Imag.* 27 (2018) 53–61.
- [19] B. Quesson, J.A. de Zwart, C.T. Moonen, Magnetic resonance temperature imaging for guidance of radiotherapy, *J. Magn. Reson. Imag. : JMRI* 12 (2000) 525–533.
- [20] K.K. Vigen, J. Jarrard, V. Rieke, J. Frisoli, B.L. Daniel, K. Butts Pauly, In vivo porcine liver radiofrequency ablation with simultaneous MR temperature imaging, *J. Magn. Reson. Imag. : JMRI* 23 (2006) 578–584.
- [21] A. Farashahi, A. Zare-Sadeghi, A. Shakeri-Zadeh, S. Kamran Kamrava, S. Maleki, H. Ghaznavi, F. Faeghi, Real-time mapping of heat generation and distribution in a laser irradiated agar phantom loaded with gold nanoparticles using MR temperature imaging, *Photodiagnosis Photodyn. Ther.* 25 (2019) 66–73.
- [22] M. Asadi, J. Beik, R. Hashemian, S. Laurent, A. Farashahi, M. Mobini, H. Ghaznavi, A. Shakeri-Zadeh, MRI-based numerical modeling strategy for simulation and treatment planning of nanoparticle-assisted photothermal therapy, *Phys. Med. : PM: An. Int. J. Devoted. Appl. Phys. med. Biol. Off. J. Italian. Assoc. Biomed Phys. (AIFB).* 66 (2019) 124–132.
- [23] G. Baffou, R. Quidant, C. Girard, Heat generation in plasmonic nanostructures: influence of morphology, *Appl. Phys. Lett.* 94 (2009), 153109.
- [24] Y. Hong, E. Lee, J. Choi, S.J. Oh, S. Haam, Y.-M. Huh, D.S. Yoon, J.-S. Suh, J. Yang, Gold nanorod-mediated photothermal modulation for localized ablation of cancer cells, 2012, *J. Nanomater.* (2012), 825060.
- [25] J. Choi, J. Yang, D. Bang, J. Park, J.-S. Suh, Y.-M. Huh, S. Haam, Targetable gold nanorods for epithelial cancer therapy guided by near-IR absorption imaging, *Small* 8 (2012) 7462.
- [26] P. Mertyna, M.W. Dewhirst, E. Halpern, W. Goldberg, S. Nahum Goldberg, Radiofrequency ablation: the effect of distance and baseline temperature on thermal dose required for coagulation, *Int. J. Hyperther.* 24 (2008) 550–559.
- [27] D.T. Tu, T.T. Vu-Le, V.N. Nguyen, Q.M. Le, C.-R.C. Wnag, L.-K. Chau, T.-S. Yang, M. W.Y. Chan, C.-I. Lee, C.-C. Ting, J.-Y. Lin, H.-C. Kan, C.C. Hsu, Gold nanorods conjugated upconversion nanoparticles nanocomposites for simultaneous bioimaging, local temperature sensing and photothermal therapy of OML-1 oral cancer cells, *Int. J. Soc. Netw. Min.* 12 (1) (2021) 49–71.
- [28] A.B. Holbrook, J.M. Santos, E. Kaye, V. Rieke, K.B. Pauly, Real-time MR thermometry for monitoring HIFU ablations of the liver, *Magn. Reson. Med.: Off. J. Int. Soc. Magn. Reson. Med.* 63 (2) (2010) 365–373.